Dai, Q., Han, D., Zhuo, L., Huang, J., Islam, T., & Zhang, S. (2015). Adjustment of wind-drift effect for real-time systematic error correction in radar rainfall data. Physics and Chemistry of the Earth, 83-84, 178–186. DOI: 10.1016/j.pce.2015.07.006

Adjustment of wind-drift effect for real-time systematic error correction in radar rainfall data

Qiang Dai[1,2,3,*], Dawei Han[2], Lu Zhuo[2], Jing Huang[4], Tanvir Islam[5, 6], Shuliang Zhang[1, 3]

[1]Key Laboratory of VGE of Ministry of Education, Nanjing Normal University, Nanjing, China

[2]WEMRC, Department of Civil Engineering, University of Bristol, Bristol, UK

[3]Jiangsu Center for Collaborative Innovation in Geographical Information Resource Development and Application, Nanjing Normal University, Nanjing, China

[4]State Key Laboratory of Hydrology-Water Resources and Hydraulic Engineering, Hohai University, China

[5]NOAA/NESDIS Center for Satellite Applications and Research, College Park, MD, USA

[6]Cooperative Institute for Research in the Atmosphere, Colorado State University, Fort Collins, Colorado, USA

***Corresponding author:**

Qiang Dai

Water and Environmental Management Research Centre

University of Bristol

93 Woodland Road

Bristol, BS8 1US, UK

E-mail: q.dai@bristol.ac.uk or dqgis@hotmail.com

Submission

Physics and Chemistry of the Earth

Abstract:

It is acknowledged that an effective bias correction procedure using gauge measurement is a significant step for radar data processing to reduce the systematic error in hydrological applications. In these bias correction methods, the spatial matching of precipitation patterns between radar and gauge network is an important premise. However, the wind-drift effect on radar measurement induces an inconsistent spatial relationship between radar and gauge measurements as the raindrops observed by radar do not fall down vertically to the ground. As a consequence, a rain gauge does not correspond to the radar pixel based on the projected location of radar beam. In this study, we introduce an adjustment method of wind-drift effect into a bias correlation scheme. We firstly simulate the trajectory of raindrops in the air using the downscaled three-dimensional wind data by the weather research and forecasting model (WRF) and calculate the final location of raindrops on the ground. The displacement of rainfall is estimated and radar-gauge spatial relationship is reconstructed. Based on this, the local real-time biases of the bin-average radar data are estimated for the selected 12 events. Then the reference mean local gauge rainfall, mean local bias and adjusted radar rainfall calculated with and without consideration of wind-drift effect are compared for different events and locations. There are considerable differences for three estimators, indicating the wind drift has a considerable impact on the real-time radar bias correction. Based on these facts, we suggest bias correction schemes based on the spatial correlation between radar and gauge measurements should consider the adjustment of the wind-drift effect and the proposed adjustment method is a promising solution to achieve this.

Keywords: real-time bias correction; mean local bias; radar rainfall estimates; wind drift; WRF

1. Introduction

The radar measurement has to be carefully processed to adjust a series of physical fundamental problems such as ground clutter, anomalous propagation, signal attenuation (includes radome wetting), beam blockage and vertical variability of the reflectivity (Jordan *et al.*, 2000; Ulbrich and Atlas, 2002; Michelson and Sunhede, 2004; Berne *et al.*, 2005; Anagnostou *et al.*, 2006; Campos *et al.*, 2006; Germann *et al.*, 2006; Villarini *et al.*, 2008; Villarini and Krajewski, 2010). Besides, volumetric estimation of rainwater from radar is subject to systematic bias in nature (Austin, 1987; Smith *et al.*, 1996; Dai *et al.*, 2014). After the aforementioned processes, real-time correction of bias in radar-rainfall data using reference rainfall such as rain gauge is an essential step (Collier *et al.*, 1983; Collier, 1986; Smith and Krajewski, 1991). The performance of bias correction is extremely important to hydrological applications with radar data as input or initial conditions. The real-time bias correlation schemes could be carried out for the entire study area or local domain, which are both adopted in National Weather Service (NWS) system (Hudlow, 1988; Fulton *et al.*, 1998). The mean-field correction schemes use a uniform bias for the whole study area (Smith and Krajewski, 1991; Anagnostou and Krajewski, 1998; Seo *et al.*, 1999), while the local correction schemes consider the spatial variation of radar measured bias (Wilson, 1970; Brandes, 1975; Collinge, 1991; Seo and Breidenbach, 2002).

For these bias correction methods, the spatial matching of precipitation patterns between radar and gauge network is a significant premise. However, due to the wind effects, the raindrops observed by the radar do not always fall vertically to the ground. In other words, wind can cause the drift of raindrops to induce an inconsistent spatial correlation of radar and gauge measurements. Several previous studies have realized and aimed to solve this issue (Collier, 1999; Mittermaier *et al.*, 2004; Lack and Fox, 2005; Lack and Fox, 2007; Lauri *et al.*, 2012; Dai and Han, 2014; Dai *et al.*, 2013).

But no one has considered this problem in real-time bias correction. To obtain correct spatial correlation, adjustment of wind effect on radar-gauge comparison should be carried out, which should be undertaken after the aforementioned physical processes and before bias correction. For this reason, this study integrates the wind-drift adjustment method and bias correlation scheme to present a displacement-based bias correlation. We simulate the movement of raindrops in the air using the downscaled three dimensional hourly wind data by the weather research and forecasting model (WRF). Then the final locations of radar measured raindrops on the ground are estimated, which are used to construct the new radar-gauge pairs. A real-time local bias correction method is introduced which considers the spatial and temporal sampling errors in radar and gauge measurements. The adjusted spatial relationship of radar and gauge data is used to correct the bias of radar data.

This paper is organized as follows. Section 2 describes the data and models used in this study. Section 3 introduces the adjusted method for wind-drift effects, and Section 4 describes the real-time bias correction scheme. The results and discussion of the proposed scheme are given in Section 5. Conclusions and future work are summarized in Section 6.

2. Study area and data source

Two kinds of rainfall datasets are used in this study: weather radar and dense rain gauge network available through the British Atmospheric Data Centre (BADC). The Brue catchment in Somerset, south-west England (51.08°N and 2.58°W), is chosen as the experimental catchment for this study. The maps of the Brue catchment and locations of rain gauges and radar pixels are shown in Figure 1. In the left map of Figure 1, 49 rain gauges are shown in blue dots, which are tipping bucket gauges (TBRs) with 0.2mm resolution (Dai *et al.*, 2014). There are 9×8 radar pixels in the map

with 2 km as the pixel size. Among them, 52 pixels are overlapped by the Brue catchment, and 28 pixels are covered with the most area. One can observe there are at least one rain gauge in each of 28 radar pixel cells, increasing to two gauges along two parallel southwest to northeast lines across the catchment. The radar data are from the Wardon Hill radar, located at a range around 40 km from the center of the catchment. The right map of Figure 1 shows the river network and the terrain elevation of the catchment. It can be seen from the figure that the elevation of the catchment is from about 35 m to 190 m above the sea level.

The dataset used to drive WRF model to downscale the wind data is taken from the ERA-40 reanalysis data produced by the European Centre for Medium-range Weather Forecasts (ECMWF). ERA-40 is assimilated from many sources using a three-dimensional variation assimilation system with a 6-h analysis cycle.

To evaluate the performance of the proposed scheme, 12 typical events with around 24 hour duration are chosen from the period when all the above mentioned datasets are available, which are listed in Table 1. To avoid bringing in new uncertainty, we do not adopt any methods to fill the gap if part of radar pixels or rain gauges record missing data. Table 1 shows the event ID, start, end time and duration of the events, together with the accumulated event rainfall. The accumulated values are calculated using gauge measurements. To better compare the estimated real-time biases among different events, the selected events all have fixed duration of 24 hours. To be consistent with the ECMWF data, the start and end times are set to 00, 06, 12 and 18 UTC.

3. Adjustment of wind drift effect

To adjust the inconsistent spatial relationship between radar and gauge measurements, we need to simulate the trajectory of raindrop observed by radar and its final location on the ground. There

are four major factors that influence the magnitude of the wind-drift effect: three-dimensional wind field from radar beam to the ground; the distance of the study area to the radar; the type of hydrometeors and the radar and gauge rainfall accumulation periods. The detailed algorithm works as follows:

In the first step, we divide the space between the ground surface and radar beam into multiple vertical layers and multiple horizontal squared pixels, which are consistent to the configuration of the WRF model. In such a way the individual atmospheric element is assumed as uniform within a sub-space. There are two initial conditions that are to be configured. The initial diameter of raindrop can be derived from the drop size distribution (DSD), and the normalized gamma DSD is adopted in this study. In addition, the initial raindrop position includes the horizontal coordinates and the vertical height. The former is set to the center point of each radar pixel and the latter uses the center beam height. The derivation of the initial information is discussed by Dai *et al.* (2013).

The movements of raindrops driven by gravitational force and drag forces are simulated in each sub-space by solving the particle motion equations (Choi, 1997). The trajectories of the raindrops in each layer are computed separately as described by Dai *et al.* (2013):

$$m\frac{d^2x}{dt^2} = 6\pi\mu D\left(U - \frac{dx}{dt}\right)\frac{C_d R_e}{24}$$

$$m\frac{d^2y}{dt^2} = 6\pi\mu D\left(V - \frac{dy}{dt}\right)\frac{C_d R_e}{24} \tag{1}$$

$$m\frac{d^2\eta}{dt^2} = 6\pi\mu D\left(W - \frac{d\eta}{dt}\right)\frac{C_d R_e}{24} - mg\left(1 - \frac{\rho_a}{\rho_w}\right)$$

where m and D represent the raindrop mass and diameter, R_e is the Reynolds number, ρ_a and ρ_w refer to the densities of air and water respectively, μ is the air viscosity, C_d denotes the drag coefficient on the raindrop. U, V and W are the x-, y- and η-components of the wind field respectively. The numerical simulation process is performed in each time step, which is iterated until the raindrops move out of the sub-space. Then the simulation is performed in the new sub-space. The final location on the ground is named as revised raindrop points (RRPs), whose coordinates ($X_{i,R}$, $Y_{i,R}$) for pixel i are obtained using:

$$X_{i,R} = X_{i,O} + \sum_{k=1}^{kn} dx_{i,k} \tag{2}$$

$$Y_{i,R} = Y_{i,O} + \sum_{k=1}^{kn} dy_{i,k} \tag{3}$$

where ($X_{i,O}$, $Y_{i,O}$) are the original horizontal coordinates of raindrops (ORP). $dx_{i,k,}$ and $dy_{i,k}$ are the displacements for layer k in the x and y directions respectively. kn denotes the layer number. Thus we obtain the final positions on the ground of the observed raindrops by radar. Only short description of the algorithm is given here, and the interested reader can refer to Dai *et al*. (2013) and Dai and Han (2014) for more information.

4. Real-time correction of bias in radar data

The procedure of real-time bias correction includes three steps. Firstly, the point rain gauge measurement is estimated for the areal rainfall. Then local bias is calculated for each event and radar pixel. Finally, the bias is used to adjust the original radar measurement. More specifically, to describe the spatially nonuniform bias in radar-rainfall data, we define the real-time local bias with the center location of each radar pixel at (x_0, y_0) as:

$$\beta(x_0, y_0, k) = \frac{G(x_0, y_0, k)}{R(x_0, y_0, k)} \tag{4}$$

where G and R refer to the hourly accumulations of pixel-averaged gauge and radar data at time k respectively. As the gauge only measures rainfall at one point, the pixel-averaged gauge data refer to the spatial average at the center of radar pixel. On the contrary, radar measures areal rainfall at one time step, so pixel-averaged radar data represents the temporal average at time k. Equation (4) can be rewritten to:

$$\beta(x_0, y_0, k) = \frac{A(x_0, y_0)^{-1} \int_A G(x_n, y_n, k)}{\int_T R(x_0, y_0, t)} \tag{5}$$

where (x_n, y_n) refers to each gauge location located within the given domain with $A(x_0, y_0)$ as the area and n as the gauge index. The domain A represent the search area. T denotes the duration of accumulations and t refers to the time step. Traditionally, the spatial matching between radar and gauge is based on their horizontal coordinates. As shown in Figure 2, a blue circle centered at the center point of a radar pixel (ORP) contains three rain gauges, which are called highlighted rain gauges. The radius of the circle is called the search distance. However, due to the wind-drift effects, the rainfall observed by radar at ORP drifts to a new location (RRP), say, the red point in Figure 2. The location of RRP is calculated based on the algorithm in Section 3. The rain gauges engaged in Equation (5) change to a new group. In Figure 2, they are highlighted in orange. The other radar-gauge spatial relationship should also be changed in the same way with the consideration of wind drift. In fact, the area of the sampled rain gauges should be equal to the area of the radar pixel. The Brue catchment is designed to configure at least one rain gauge at each of its 28 radar pixels. But due to the wind-drift effects, this condition is no longer satisfied as the spatial relationship between

radar and gauge is changed. As a consequence, many radar pixels may have no corresponding rain gauges. So the area of the search circle is set to be a bit larger than the radar pixel to enable radar pixels to contain at least one rain gauge for most situations.

To implement the bias correction, we define a Spatial Correction Matrix (SCM) that describes the spatial connections of all radar pixels and rain gauges. For each radar pixel, SCM illustrates whether it has a relationship with each rain gauge. Values equal to 1 mean the radar pixel and the gauge are related to each other, and these equal to 0 mean no correlation. The row and column numbers of SCM correspond to the number of radar pixels and rain gauges. Without considering the wind drift, SCM is fixed and determined only by the separated distances among radar pixels and rain gauges. On the contrary, SCM varies with each event when taking account of wind-drift effect.

As gauge measures continuous rainfall at a point, it is subject to spatial sampling. Radar rainfall has to be sampling at space and time, so it is subject to both spatial and temporal sampling errors. For this reason, Equation (4) should be average over time to obtain an unbiased estimate of bias. The local bias estimator is written as:

$$\beta^*(x_0, y_0, k) = \frac{E[G(x_0, y_0, k)]}{E[R(x_0, y_0, k)]} \tag{6}$$

To harmonize the calculation of displacement of raindrops and real-time bias correction, all events selected in this study cover a period of 24 hours. Local bias in Equation (6) is averaged over the given fix window (24 hours). The estimated local bias is then multiplied with the radar rainfall measurement at a given location and event to obtain the adjusted radar estimate.

5. Results and discussion

5.1 Derivation of three-dimensional wind data

The derivation of three-dimensional wind data by WRF is the first step in simulating the trajectory of raindrops in the air. The WRF model is configured with three nested domains. The finest spatial and temporal resolutions of WRF are set to 3.3 km and 1 hour. Pixel numbers, domain sizes and downscaling ratios of three domains are listed in Table 2. To obtain detailed variation of the vertical wind field, 28 layers are configured on a hydrostatic-pressure vertical coordinate system. As the derivation of wind data is a fundamental component of WRF, we adopt the commonly used settings of major WRF physical schemes, such as microphysics, cumulus, planetary boundary, land surface model, shortwave radiation and longwave radiation schemes. The schemes used in this study together with their references are listed in Table 3 (Dai *et al.*, 2013). The model is run for 12 chosen events and the wind data is extracted from the output NetCDF file.

5.2 Simulation of raindrops trajectory in the air

The trajectory of raindrops in the air is simulated and their final location on the ground is estimated based on the proposed algorithm. Figure 3 displays the estimated displacements of raindrops under the wind-drift effect for Event 1 (05/01/1994). The orange dots are the centered locations of radar pixels, while the red ones are their adjusted positions. There are four time steps drawn in the figure. It is clear that different patterns of drift directions and distances can be observed in one event. For Figures 3 (a) and (b), the drift distances are quite large, covering two or almost three radar pixels. On the contrary, the drift distances are relatively small in Figure 3 (c) and the RRPs are almost in the same pixel as ORPs. In the same time step, there is also a considerable variation of drift distances and directions for different radar pixels. Take Figure 3 (b) for example, the drift distances

in northern pixels (e.g. three pixels with center Northing coordinates of 141 km) are larger than those in southern part (e.g. two pixels with center Northing coordinates of 131 km).

Table 4 details the estimated results and information of ground measurements for Event 1. The ground measurements include mean gauge rainfall, ground wind direction and wind speed. All statistics are averaged values for the study area. The ground winds represent ones at 2 m height. The drift directions and distances are the mean values of the 28 radar pixels. The drift distance is mainly determined by rainfall intensity and three-dimensional wind from the radar beam to the ground. Comparing the drift distance to the ground wind speed, one can observe a possible relation between them. For example, the largest drift distance is 2.6 km at 12:00 of the event, and the wind speed is the strongest at the same time. In addition, the drift distances are quite small (0.9 and 0.7 km) at time 20:00 and 21:00, and their corresponding ground wind speeds are very weak (1.3 and 1.2 m/s) as well. However, this is not true for all the time steps. A strong ground wind is observed at 07:00 (3.2 m/s), while the induced drift distance is only 1.8 km. Therefore, the ground wind data can only partially reflect the wind drift effects, but cannot substitute the three-dimensional wind field from the radar beam to the ground. In terms of the relationship between rainfall intensity and drift distance, a weaker relation is observed. At time 12:00, although the rainfall intensity is very small (0.27 mm), the drift distance is quite large just because the wind speed is strong. Finally, for drift direction, no clear pattern can be found with the comparison to the ground wind direction, indicating the ground data cannot replace the three-dimensional wind field.

5.3 Bias correction using the adjusted radar-gauge pairs

With the drift locations of radar pixels, we can reassign the new radar-gauge pairs for real-time bias correction of radar data. The estimated results are shown in Figures 4 and 5. The procedure

includes three sub-processes: estimation of the mean rainfall values of the highlighted gauges; estimation of the local bias and adjustment of the radar rainfall. In Figures 4 and 5, we display the mean rainfall values of the highlighted gauges with and without consideration of wind drift for radar Pixels 1 (Easting: 365 km, Northing: 141 km) and 15 (Easting: 361 km, Northing: 135 km) respectively. Radar Pixel 1 is located in the northwest of the study area with one rain gauge inside it and only 3 rain gauges in the surrounding 8 radar pixels. On the contrary, radar Pixel 15 contains 8 rain gauges and additional 9 rain gauges in its surrounding 8 pixels. The search radius is set to 1.7 km in this study. One may observe from Figure 4 that the impact of wind drift on the mean gauge rainfall of the highlighted gauges is small for some events, such as E1, E3 and E12. However, the differences of the mean values calculated with and without consideration of wind drift are large for most events, and even show total different patterns in some events, such as E4, E5, E9 and E10. The differences between two lines are relatively small in Figure 5 for radar Pixel 15. Except some events (e.g., E8 and E9), most events are insensitive to the effects of wind drift.

Real-time local bias of radar rainfall data is calculated using Equation (6), which are shown in Figure 6 for Events 2 and 12. The left figures refer to the biases estimated based on the original radar-gauge spatial relationship, while the right ones display the estimated ones using the revised relationships. For Event 2, there are considerable changes of bias estimates in most radar pixels, especially the pixels around the boundary of the study area. There are great variations of biases among different radar pixels. The biases vary from less than 0.1 at Pixel 22 (Easting: 363 km, Northing: 133 km) to around 0.3 at Pixel 13 (Easting: 375 km, Northing: 137 km). Low bias estimate (less than 1) indicates the mean gauge measurement in the given event is quite smaller than radar measurement. In more serious cases, the radar measures rainfall while the rain gauge reports no rain. In such cases, the bias estimates are equal to zero. The majority biases in Event 12

are relatively smaller than the ones in Event 2 and most estimates are generally less than 0.2. The biases estimated with the consideration of wind-drift effect do not vary greatly compared to the original ones.

Figures 7 and 8 show the adjusted radar rainfall with and without consideration of wind drift for radar Pixels 1 and 15. The solid lines in the figures show the adjusted values based on the original local bias. The blue dots correspond to the adjusted rainfall using the revised local bias. It is observed that the peak rainfall seems to be more sensitive to the wind drift. The differences between them are huge in peak rainfall values such as Events E7, E9, E10 and E11. Among them, the adjusted rainfalls based on the original radar-gauge relationship are underestimated in Events E9 and E11, and overestimated in Events E7 and E10. The adjusted rainfall is computed by the original radar measurement multiply bias. So the peak rainfall corresponds to the large differences for the certain bias. For light rainfall, considerable changes can also be observed in Figure 7. However, the differences of the adjusted rainfall with and without consideration of wind are relatively small for Pixel 15.

6. Conclusions

Real-time bias correction based on gauge rainfall is a simple and effective way to improve the radar rainfall quality and enable it to be better applied in hydrological applications. However, the wind-drift effect induces an inconsistent spatial relationship between radar and gauge measurements. An adjusted method of wind-drift effect for real-time bias correction mechanism is proposed in this study. It firstly simulates the trajectory of raindrops in the air using the downscaled three-dimensional wind data and calculates the final location of raindrops on the ground. The displacement of rainfall is estimated and the radar-gauge spatial relationship is

reconstructed. Based on this, the local bias of the pixel-average radar data is estimated for the selected 12 events. The adjusted radar data with consideration of wind-drift effect shows different patterns compared to the ones without consideration, indicating the wind-drift effect has significant impact on real-time radar bias correction. For this reason, we suggest the procedure to lesson wind-drift effect should be introduced into the bias correlation scheme. In summary, there are two major findings in this study. Wind-drift effect can induce inconsistent spatial relationship of radar and gauge measurements, which will contaminate the process of real-time local bias correction. In addition, the simulation of raindrop trajectory can be used to reconstruct the radar-gauge spatial relationship.

Although the proposed scheme considers the influence of wind in real-time bias correction and improves the reliability of radar data, there are still some unsolved issues that require further study. Firstly, spatial and temporal sampling uncertainties have not been solved in the current bias correction. Radar scans areal rainfall at the spatial scale of 2 km in this study while rain gauge can only measure rainfall at one point (or at the scale of roughly 20 cm). We use the average value of the highlighted rain gauges to represent the estimated areal rainfall in this study. In terms of temporal scale, both radar and gauge suffer temporal sampling errors as temporal gaps exist in their measurements. The former one scans atmospheric condition every 5 minutes while the latter records the number of tips in 10-seconds intervals. The possible uncertainties due to the spatial and temporal scale discrepancies between radar and gauge measurements have been studied in the previous studies (Ciach and Krajewski, 1999; Jordan *et al.*, 2000; Villarini *et al.*, 2008) and we will investigate it in the future study. In addition, the real-time bias correlation proposed in this study reflects not only the bias when the radar successfully detected rainfall, but also when the radar observed rainfall while the gauge recorded no rain. The chosen 12 events all contain heavy

storm, so it is acceptable for this work. However, in real-time practice, the bias estimation may be strongly biased by the majority of the time steps without any precipitation. A possible solution is to calculate the mean rainfall conditioned on the occurrence of the rainy situations (Seo *et al.*, 1999; Seo and Breidenbach, 2002). Moreover, there are 49 rain gauges located in the study area, but it is not an essential condition for this study. In fact, limited rain gauges are available in most catchments. The proposed scheme should be further investigated in other areas to evaluate its performance.

Besides, there are also some unsolved problems associated with wind drift simulation. To simplify the computational process, we assume the raindrops start from the radar beam center and the movement of raindrops within each radar pixel is uniform. For the former, we have carried out sensitivity analysis to explore the effects of initial location on the simulated results in Dai *et al.* (2013). With the growth of distance to the radar location, the differences of estimated displacements using different initial locations within the beam are larger. However, we only investigate its influence on radar-gauge correlation coefficient in Dai *et al.* (2013), and the possible uncertainty introduced to radar bias correction should still be investigated. In terms of the latter assumption, the mass-weighted drop diameter should be used to calculate the trajectories of drops. In other words, the raindrops in the same pixel has the same drift distance and direction. The current scheme can only reveal the principal trajectory of raindrops. But in fact, with different distributions of rainfall and wind field within a pixel, the raindrops could move to different locations on the ground. As a consequence, the spatial relationship between radar and gauge should be reconstructed and the R-G correlation matrix is not just limited to either 0 or 1. It may be possible to tackle this issue using Agent-Based modelling. To simulate this process, a more accurate drop size distribution (DSD) is required. The DSD model has a close relation to storm

types, seasonal and atmospheric conditions. Except an accurate DSD model, the wind data with a finer spatial resolution may be required. We can explore this by configuring the WRF model to further downscale the ECMWF data.

Acknowledgements

This work was supported by the National Natural Science Foundation of China (Grant No. 41171301) and the PAPD program (164320H116). The authors acknowledge the British Atmospheric Data Centre and the European Centre for Medium-range Weather Forecasts for providing the data.

References

Anagnostou EN, Krajewski WF. 1998. Calibration of the WSR-88D precipitation processing subsystem. Weather and forecasting, **13**: 396-406.

Anagnostou MN, Anagnostou EN, Vivekanandan J. 2006. Correction for rain path specific and differential attenuation of X-band dual-polarization observations. Geoscience and Remote Sensing, IEEE Transactions on, **44**: 2470-2480.

Austin PM. 1987. Relation between measured radar reflectivity and surface rainfall. Monthly Weather Review, **115**: 1053-1070.

Berne A, Delrieu G, Andrieu H. 2005. Estimating the vertical structure of intense Mediterranean precipitation using two X-band weather radar systems. Journal of Atmospheric and Oceanic Technology, **22**: 1656-1675.

Brandes EA. 1975. Optimizing rainfall estimates with the aid of radar. Journal of Applied Meteorology, **14**: 1339-1345.

Campos E, Zawadzki I, Petitdidier M, Fernandez W. 2006. Measurement of raindrop size distributions in tropical rain at Costa Rica. Journal of Hydrology, **328**: 98-109.

Chen F, Dudhia J. 2001, Coupling an advanced land surface-hydrology model with the Penn State-NCAR MM5 modeling system. Part I: Model implementation and sensitivity, Monthly Weather Review, **129**: 569-585.

Choi E. 1997. Numerical modelling of gust effect on wind-driven rain. Journal of Wind Engineering and Industrial Aerodynamics, **72**: 107-116.

Ciach GJ, Krajewski WF. 1999. On the estimation of radar rainfall error variance. Advances in Water Resources, **22**: 585-595.

Collier C. 1986. Accuracy of rainfall estimates by radar, Part I: Calibration by telemetering raingauges. Journal of Hydrology, **83**: 207-223.

Collier C. 1999. The impact of wind drift on the utility of very high spatial resolution radar data over urban areas. Physics and Chemistry of the Earth, Part B: Hydrology, Oceans and Atmosphere, **24**: 889-893.

Collier C, Larke P, May B. 1983. A weather radar correction procedure for real‐time estimation of surface rainfall. Quarterly Journal of the Royal Meteorological Society, **109**: 589-608.
Collinge V. 1991. Weather radar calibration in real time: prospects for improvement. Hydrological Applications of Weather Radar, Ellis Horwood, London: 25-42.
Dai Q, Han D. 2014. Exploration of discrepancy between radar and gauge rainfall estimates driven by wind fields, Water Resource Research, **50**: 8571–8588,.
Dai Q, Han D, Rico-Ramirez MA, Islam T. 2013. The impact of raindrop drift in a three-dimensional wind field on a radar–gauge rainfall comparison. International Journal of Remote Sensing, **34**: 7739-7760.
Dai Q, Han D, Rico Ramirez MA, Srivastava PK. 2014. Multivariate Distributed Ensemble Generator: A new scheme for ensemble radar precipitation estimation over temperate maritime climate. Journal of Hydrology, **511**: 17-27.
Dudhia J. 1989, Numerical study of convection observed during the winter monsoon experiment using a mesoscale two-dimensional model, Journal of the Atmospheric Sciences, **46**: 3077-3107.
Fulton RA, Breidenbach JP, Seo D-J, Miller DA, O'Bannon T. 1998. The WSR-88D rainfall algorithm. Weather and Forecasting, **13**: 377-395.
Germann U, Galli G, Boscacci M, Bolliger M. 2006. Radar precipitation measurement in a mountainous region. Quarterly Journal of the Royal Meteorological Society, **132**: 1669-1692.
Hudlow MD. 1988. Technological developments in real-time operational hydrologic forecasting in the United States. Journal of Hydrology, **102**: 69-92.
Hong SY, Dudhia J, Chen SH. 2004, A revised approach to ice microphysical processes for the bulk parameterization of clouds and precipitation, Monthly Weather Review, **132**: 103–120.
Hong SY, Noh Y, Dudhia J. 2006, A new vertical diffusion package with an explicit treatment of entrainment processes, Monthly Weather Review, **134**: 2318–2341.
Jordan P, Seed A, Austin G. 2000. Sampling errors in radar estimates of rainfall. Journal of Geophysical Research: Atmospheres (1984–2012), **105**: 2247-2257.
Kain JS. 2004, The Kain–Fritsch convective parameterization: an update, Journal of Applied Meteorology, **43**: 170–181.
Lack SA, Fox NI. 2005. Errors in surface rainfall rates retrieved from radar due to wind‐drift. Atmospheric Science Letters, **6**: 71-77.
Lack SA, Fox NI. 2007. An examination of the effect of wind-drift on radar-derived surface rainfall estimations. Atmospheric research, **85**: 217-229.
Lauri T, Koistinen J, Moisseev D. 2012. Advection-Based Adjustment of Radar Measurements. Monthly Weather Review, **140**.
Michelson DB, Sunhede D. 2004. Spurious weather radar echo identification and removal using multisource temperature information. Meteorological Applications, **11**: 1-14.
Mittermaier MP, Hogan RJ, Illingworth AJ. 2004. Using mesoscale model winds for correcting wind‐drift errors in radar estimates of surface rainfall. Quarterly Journal of the Royal Meteorological Society, **130**: 2105-2123.
Mlawer EJ, Taubman SJ, Brown PD, Iacono MJ, Clough SA. 1997, Radiative transfer for inhomogeneous atmospheres: RRTM, a validated correlated‐k model for the longwave, Journal of Geophysical Research: Atmospheres (1984‐2012), **102**: 16663-16682.

Seo D-J, Breidenbach J. 2002. Real-time correction of spatially nonuniform bias in radar rainfall data using rain gauge measurements. Journal of Hydrometeorology, **3**: 93-111.
Seo D-J, Breidenbach J. 2002. Real-time correction of spatially nonuniform bias in radar rainfall data using rain gauge measurements. Journal of Hydrometeorology, **3**.
Seo D-J, Breidenbach J, Johnson E. 1999. Real-time estimation of mean field bias in radar rainfall data. Journal of Hydrology, **223**: 131-147.
Smith JA, Krajewski WF. 1991. Estimation of the mean field bias of radar rainfall estimates. Journal of Applied Meteorology, **30**: 397-412.
Smith JA, Seo DJ, Baeck ML, Hudlow MD. 1996. An intercomparison study of NEXRAD precipitation estimates. Water Resources Research, **32**: 2035-2045.
Ulbrich CW, Atlas D. 2002. On the separation of tropical convective and stratiform rains. Journal of Applied Meteorology, **41**: 188-195.
Villarini G, Krajewski WF. 2010. Review of the different sources of uncertainty in single polarization radar-based estimates of rainfall. Surveys in Geophysics, **31**: 107-129.
Villarini G, Mandapaka PV, Krajewski WF, Moore RJ. 2008. Rainfall and sampling uncertainties: A rain gauge perspective. Journal of Geophysical Research: Atmospheres (1984–2012), **113**.
Wilson JW. 1970. Integration of radar and raingage data for improved rainfall measurement. Journal of Applied Meteorology, **9**: 489-497.

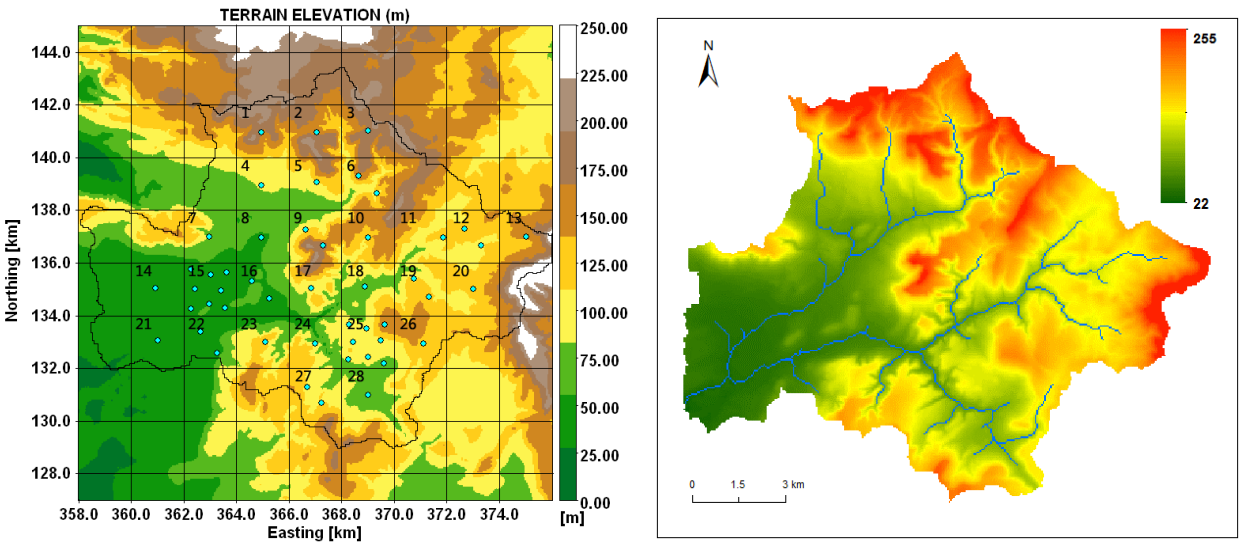

Figure 1. Maps of the study area. The left map shows the rain gauge network and radar pixels (2×2 km). The indexes of the radar pixels are labeled in the map. The circle dots represent the rain gauge locations. The right map displays the rive network and the terrain elevation of the catchment. Both maps are drawn based on the British National Pixel coordinate system.

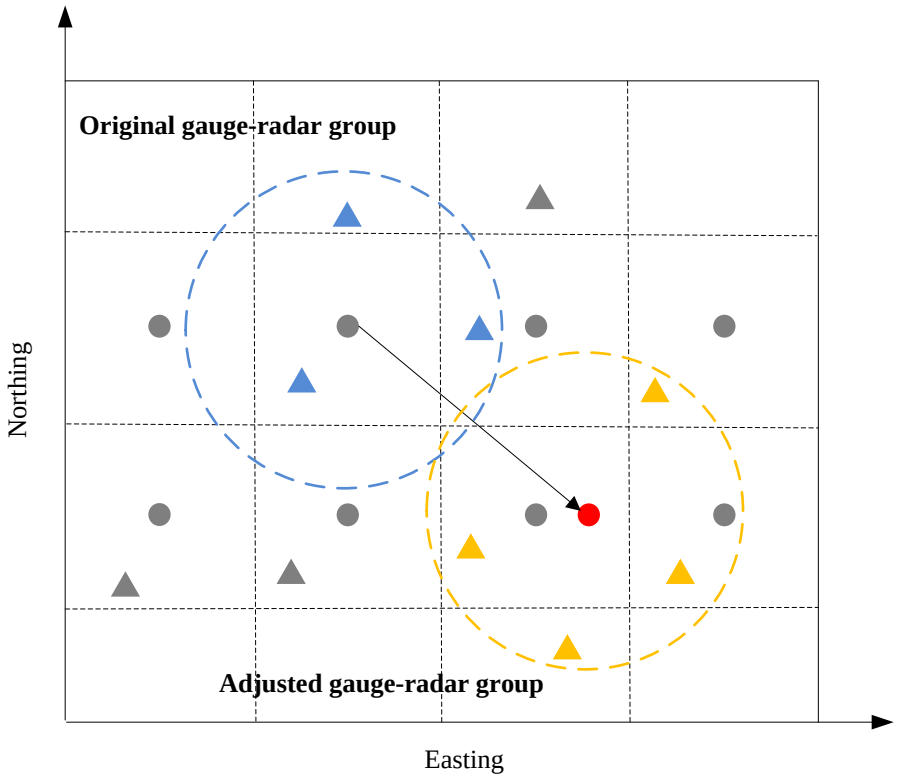

Figure 2. A schematic chart of the effect of wind-drift on the spatial relationship among radar pixels and rain gauges. The solid points refer to the center of radar pixels while the triangles represent the rain gauges. Due to the wind drift, the raindrops observed by radar move to a new location, which is drawn as a red point.

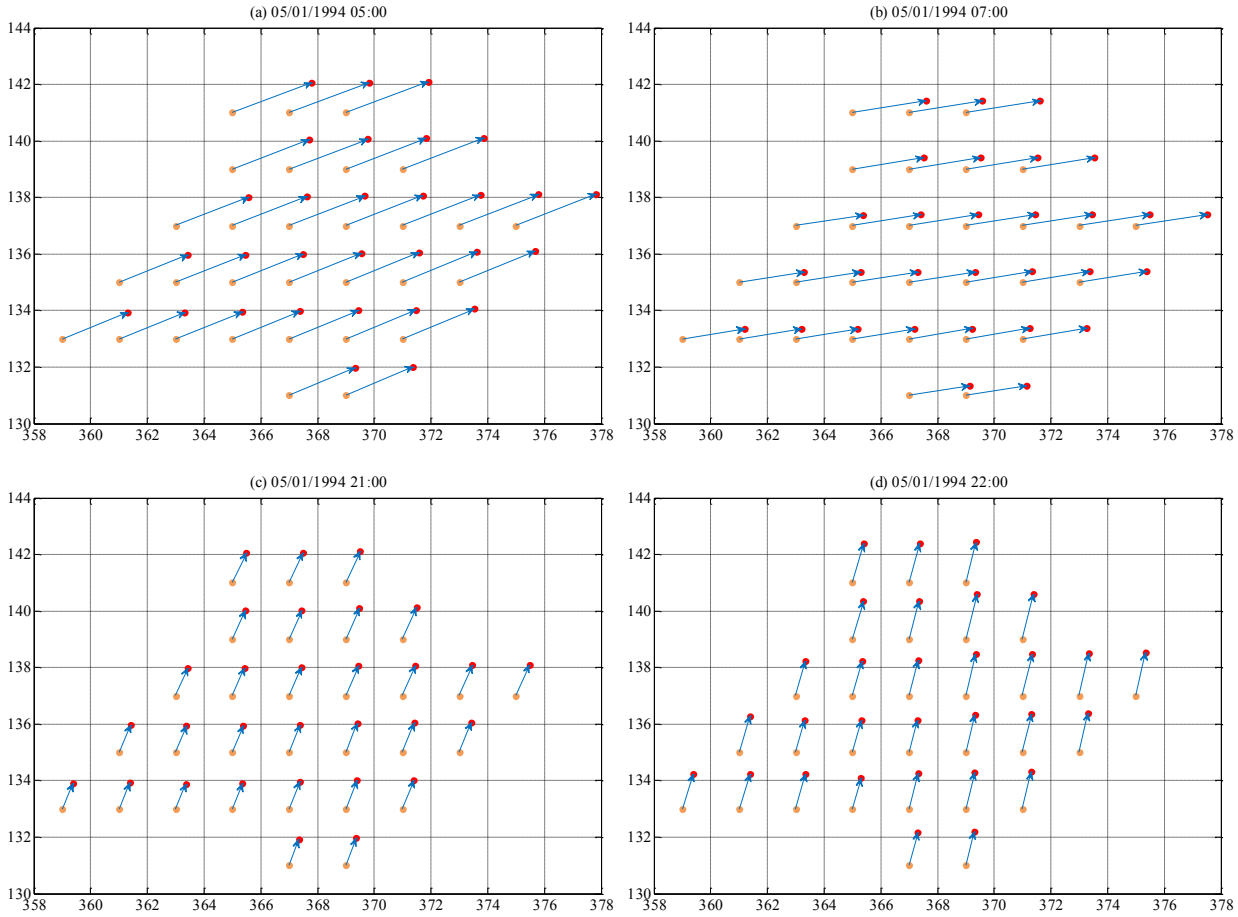

Figure 3. The estimated displacements of raindrops under the effects of wind-drift for Event 1 (05/01/1994). The orange dots are the locations of radar pixel centers, while the red ones are their adjusted positions.

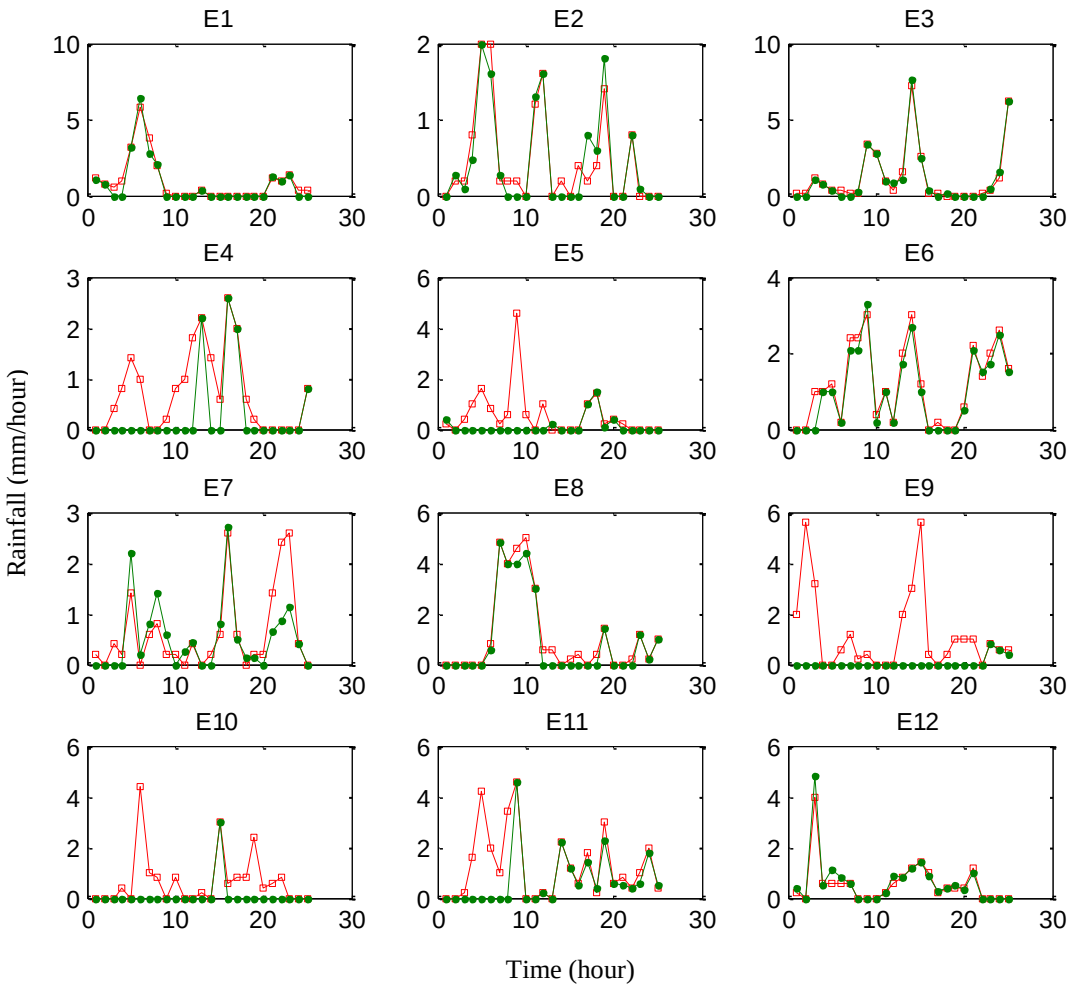

Figure 4. The mean rainfalls of highlighted gauges with (red squares line) and without (green points line) consideration of wind drift for the radar Pixel 1 (Easting: 365 km, Northing: 141 km).

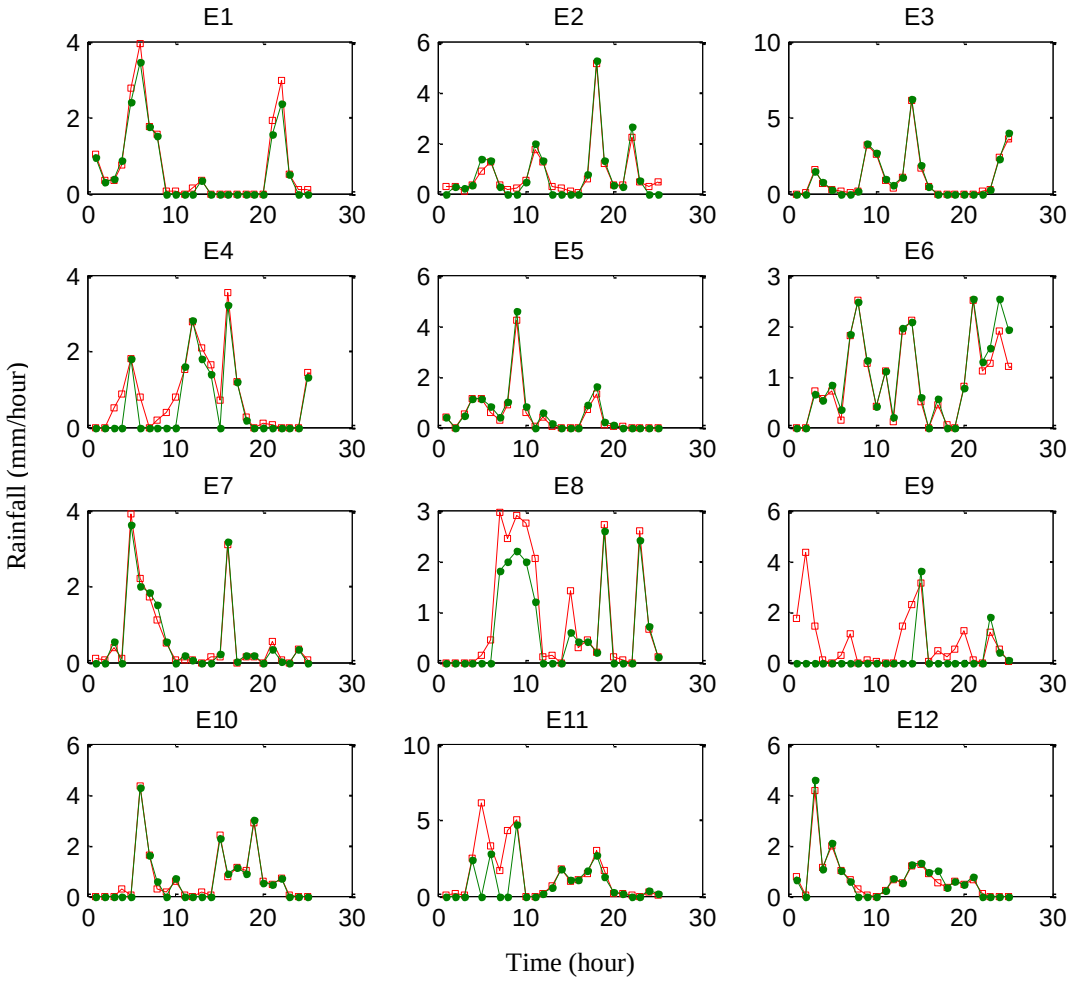

Figure 5. The same as Figure 4 but for Pixel 15 (Easting: 361 km, Northing: 135 km).

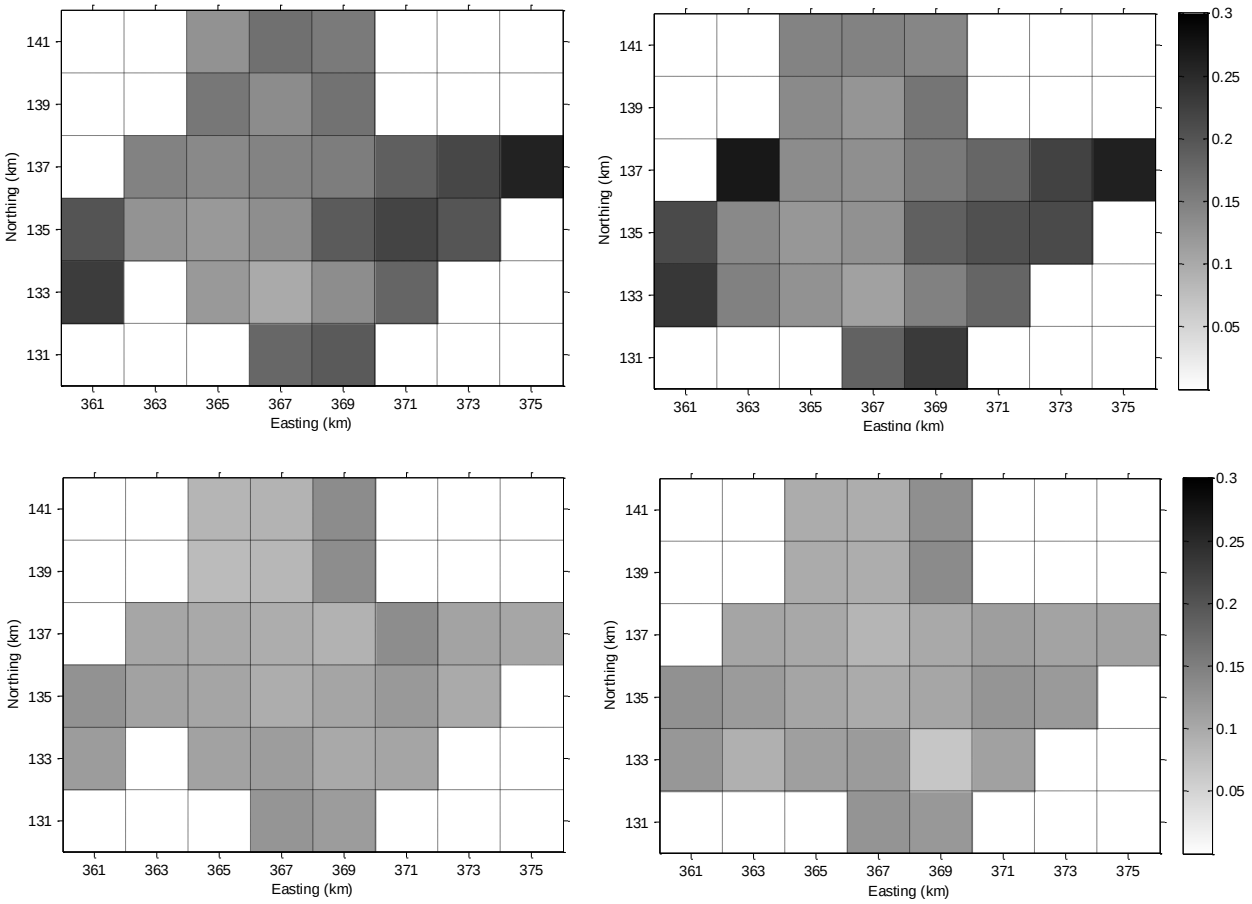

Figure 6. The real-time local bias of radar rainfall data for Events 2 and 12. The left two figures refer to the biases estimated using the original radar-gauge spatial relationship, and right ones display the estimated ones using the revised spatial relationships.

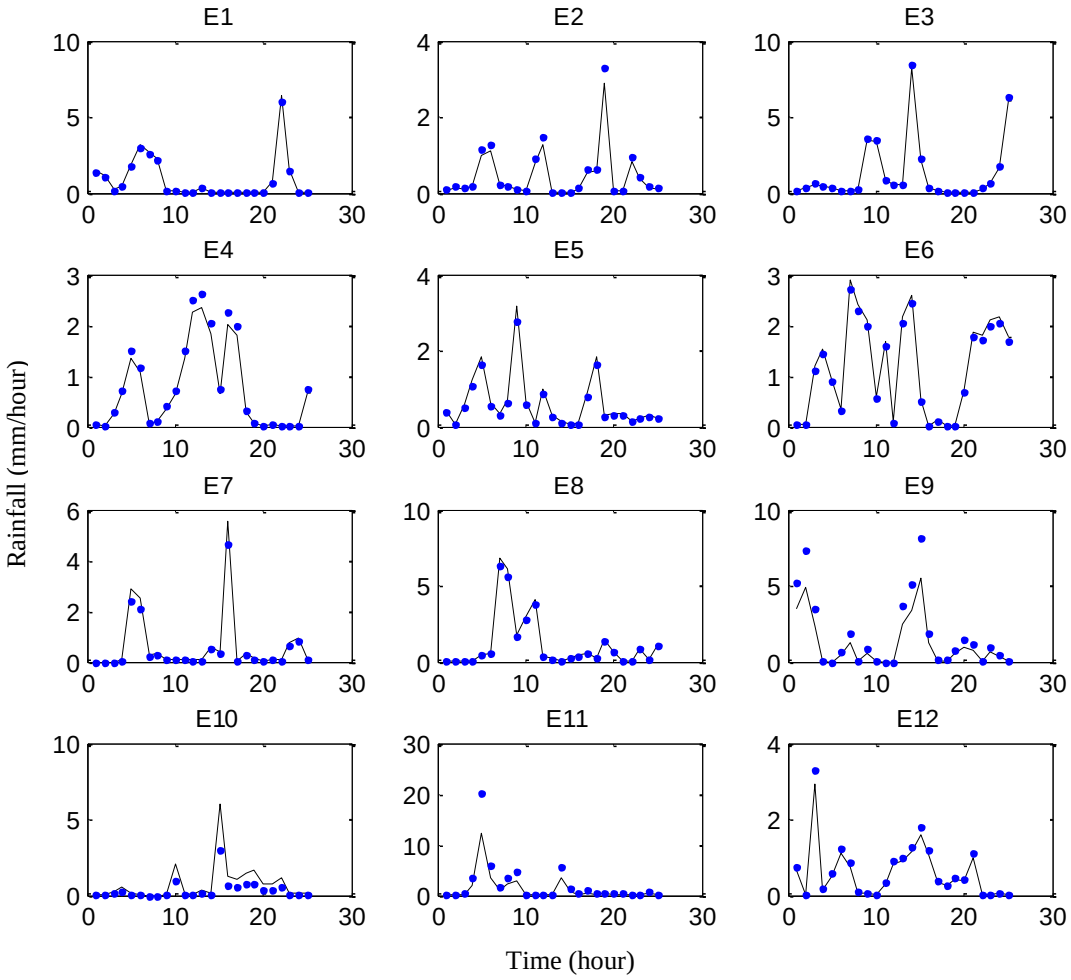

Figure 7. The adjusted radar rainfall with (blue points) and without (solid line) consideration of the wind-drift effect for the radar Pixel 1 (Easting: 365 km, Northing: 141 km).

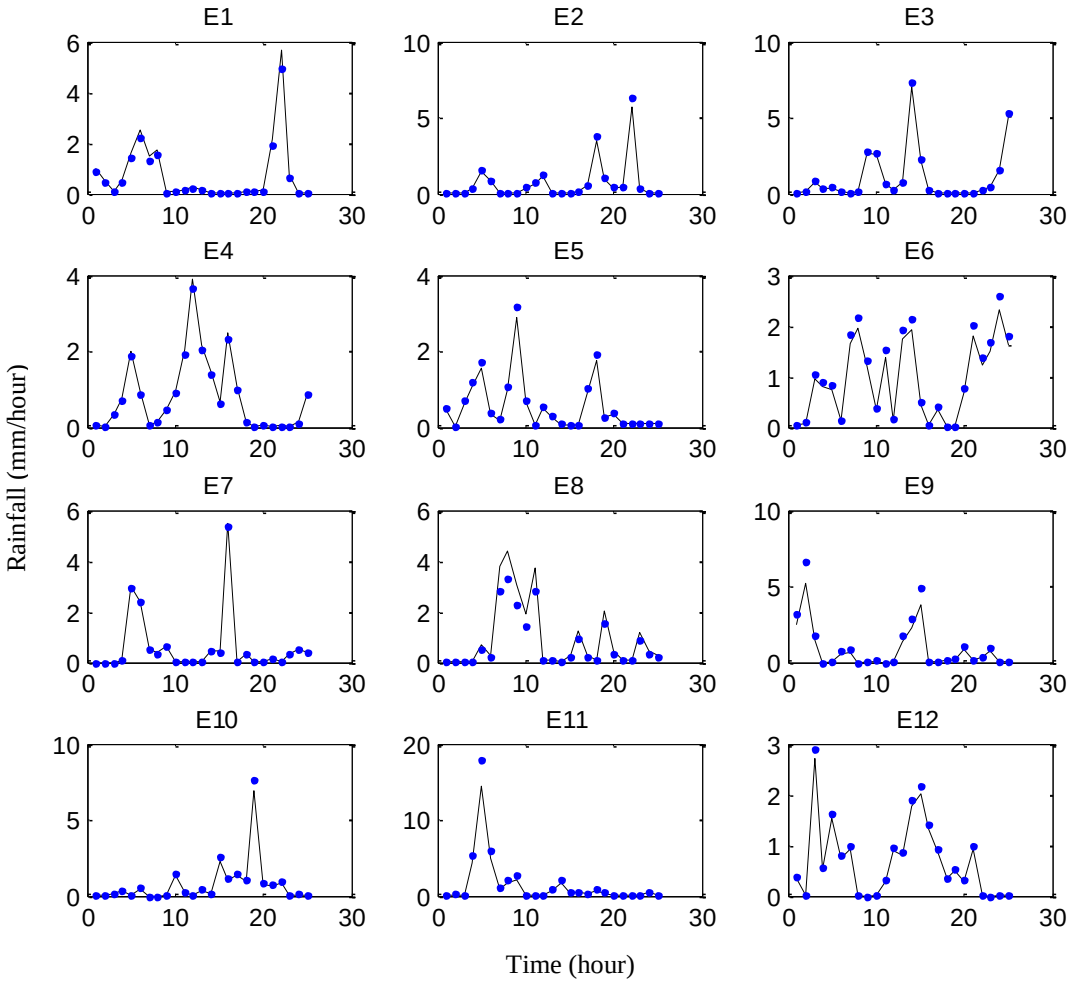

Figure 8. The same as Figure 7 but for Pixel 15 (Easting: 361 km, Northing: 135 km).

Table 1. Information of the selected events. The accumulated rainfall is the averaged gauge measurements in the Brue catchment.

Event ID	Storm start time	Storm end time	Accumulated Rainfall (mm)
1	1994-01-05:00	1994-01-06:00	20.24
2	1994-05-21:18	1994-05-22:18	24.90
3	1994-10-29:12	1994-10-30:12	41.96
4	1994-11-08:12	1994-11-09:12	35.51
5	1994-12-08:00	1994-12-09:00	16.20
6	1994-12-27:00	1994-12-28:00	30.09
7	1995-02-22:12	1995-02-23:12	14.74
8	1995-04-22:00	1995-04-23:00	24.37
9	1995-09-06:18	1995-09-07:18	29.20
10	1995-11-26:12	1995-11-27:12	16.60
11	1996-11-19:00	1996-11-20:00	34.55
12	1997-08-24:12	1997-08-25:12	19.01

Table 2. The WRF model configuration for the three nested domains.

Domain	Pixel spacing (km)	Pixel number	Domain size (km)	Downscaling ratio
Domain1	30	18×18	540×540	
Domain2	10	19×19	190×190	1:3
Domain3	3.3	22×22	73×73	1:3

Table 3. The physical schemes used in the WRF model.

Items	Parameters/schemes	References
Dynamics solvers	ARW	-
Microphysics scheme	WRF single-moment three class	*Hong et al*. [2004]
Cumulus Parameterisation scheme	Kain-Fritsch	*Kain* [2004]
Planetary boundary scheme	Yonsei university scheme	*Hong et al*. [2006]
Land surface model	Noah model	*Chen and Dudhia* [2001]
Shortwave radiation scheme	Dudhia model	*Dudhia* [1989]
Longwave radiation scheme	Rapid radiative transfer model	*Mlawer et al*. [1997]

Table 4. The information of ground measurements and adjusted values of wind-drift for Event 1 (05/01/1994). All statistics are averaged values for the study area.

Time	Rainfall (mm)	Ground wind direction (^{0})	Ground wind speed (m/s)	Drift direction (^{0})	Drift distance (km)
05/01 01:00	0.52	161	1.9	69	1.7
05/01 05:00	4.01	214	2.8	22	2.0
05/01 06:00	2.57	252	2.8	17	2.0
05/01 07:00	2.13	258	3.2	9	1.8
05/01 12:00	0.27	249	4.2	8	2.6
05/01 20:00	2.29	86	1.3	58	0.9
05/01 21:00	2.77	144	1.2	67	0.7
05/01 22:00	0.69	77	1.1	75	1.1